INTERNATIONAL JOURNAL FOR NUMERICAL METHODS IN FLUIDS
Int. J. Numer. Meth. Fluids 2003; **42**:765–790 (DOI: 10.1002/fld.553)

A new VOF-based numerical scheme for the simulation of fluid flow with free surface. Part I: New free surface-tracking algorithm and its verification

Min Soo Kim[1] and Woo Il Lee[2,*,†]

[1]*MEMS Lab, Samsung Advanced Institute of Technology, P.O. Box 111, Suwon 440-600, Korea*
[2]*School of Mechanical and Aerospace Engineering, Seoul National University, Seoul 151-742, Korea*

SUMMARY

Numerical simulation of fluid flow with moving free surface has been performed. For the free surface flow, a volume of fluid (VOF)-based algorithm utilizing a fixed grid system has been investigated. In order to reduce numerical smearing at the free surface represented on a fixed grid system, a new free surface-tracking algorithm based on the donor–acceptor scheme has been proposed. Novel features of the proposed algorithm are characterized by two numerical tools; the orientation vector to represent the free surface orientation in each cell and the baby-cell to determine the fluid volume flux at each cell boundary. The proposed algorithm can be easily implemented in any irregular non-uniform grid systems usually encountered in the finite element method (FEM). Moreover, the proposed algorithm can be extended and applied to the 3D free surface flow problems without additional efforts. For computation of unsteady incompressible flow, a finite element approximation based on the explicit fractional step method has been adopted. In addition, the streamline upwind/Petrov–Galerkin (SUPG) method has been implemented to deal with convection dominated flows. Combination of the proposed free surface-tracking scheme and the explicit fractional step formulation resulted in an efficient solution algorithm. Validity of the present solution algorithm was demonstrated from its application to the broken dam and the solitary wave propagation problems. Copyright © 2003 John Wiley & Sons, Ltd.

KEY WORDS: free surface; volume of fluid (VOF) method; orientation vector; baby-cell; fixed grid system; fractional step method

1. INTRODUCTION

When the free surface flow is analysed numerically, two problems should be addressed. One is to identify the free surface location at present time step and the other is to update the

*Correspondence to: W. I. Lee, School of Mechanical and Aerospace Engineering, Seoul National University, San 56-1, Shinlim-dong, Kwanak-ku, Seoul 151-742, Korea.
†E-mail: wilee@snu.ac.kr

Contract/grant sponsor: Brain Korea-21
Contract/grant sponsor: Korea Ministry of Science and Technology

Received 3 November 2000
Revised 11 March 2003

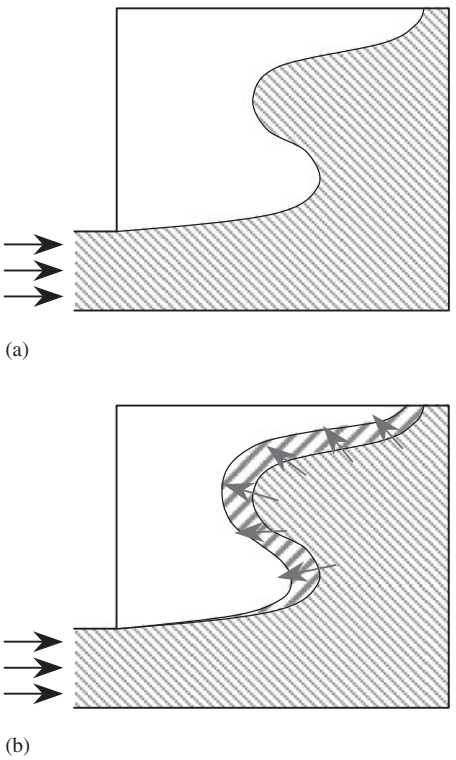

Figure 1. Numerical analysis of fluid flow with moving free surface. Difficulties arise from the problems associated with: (a) identifying and (b) update of free surface location.

location at the next time step for a given flow field (see Figure 1). In order to trace the moving free surface, a number of methods have been proposed. Those can be categorized into two groups, i.e. moving grid method and fixed grid method [1]. In the moving grid method, also known as the Lagrangian method [2–5], grid points are embedded in the fluid and move with it (see Figure 2(a)). The fluid always coincides with the region to be analysed and each computational cell contains the same fluid elements. Therefore, free surface can be delineated specifically and can be traced precisely. Also, free surface boundary conditions can be applied on the exact material interfaces. However, many problems with the complicated geometry may occur. The Lagrangian method is apt to fail when the fluid undergoes large deformation. Mesh may become highly distorted and cause numerical inaccuracy in the solution of the flow field. Furthermore, the number of grid points changes and thus remeshing or rezoning process should be carried out after each movement or several movements of the free surface, resulting in large computation time. On the other hand, to avoid shortcomings associated with severe mesh distortion in the Lagrangian methods, an algorithm implementing a continuous rezoning process has been proposed. The algorithm is referred as the arbitrary Lagrangian–Eulerian (ALE) method [6]. The ALE method allows the grid points to move with a relative velocity with respect to the fluid [7–9].

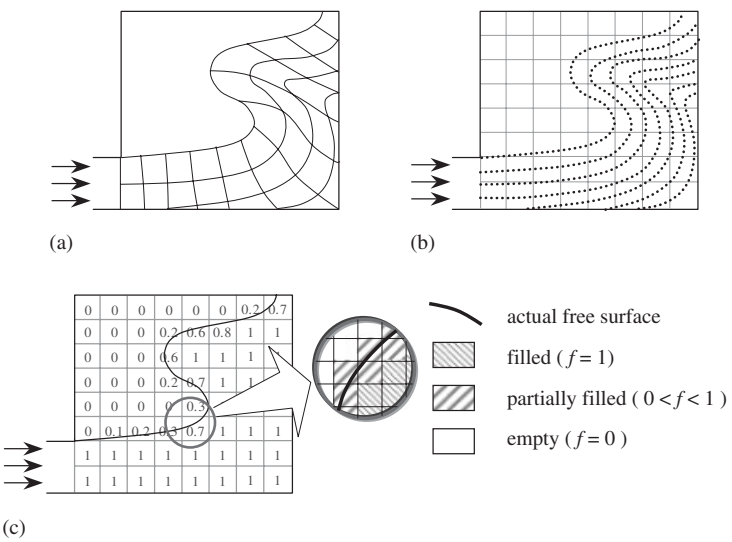

Figure 2. Numerical methods for the fluid flow with moving free surface. Moving grids: (a) Lagrangian method, and fixed grids, (b) MAC method and (c) VOF method.

In the fixed grid method, also called the Eulerian method, mesh is treated as a fixed reference frame through which the fluid moves. The initially generated mesh is used throughout the entire computation and thus no geometric difficulty arises. Therefore, the fixed grid method can remarkably reduce computational efforts compared to the moving grid method. Furthermore, it facilitates easy extension to the 3D problems. However, the fixed grid method has some shortcomings associated with determination of free surface location. The nodal points are fixed at their initial positions and the free surface is located between some of them. Therefore, the free surface is liable to lose its intrinsic nature of sharp discontinuity and thus special schemes are required to avoid the numerical smearing. Volume tracking method is known as the numerical technique which has a potential of dealing with large free surface deformation on the fixed grids. Two methods have been widely accepted (see Figures 2(b) and (c)): the marker and cell (MAC) method [10–15] and the volume of fluid (VOF) method [16–33]. In the VOF method, free surface location is determined by solving a transport equation for a parameter representing the fractional fluid volume in a cell. Along with a number of VOF-based algorithms, several schemes have been also proposed to avoid the phenomenon of numerical smearing. However, some schemes proposed are very complicated even for 2D problems and, in some cases, result in excessive numerical smearing on the free surface. Consequently, there has been an increasing demand for a simple and efficient free surface-tracking algorithm that can deal with large free surface motion with minimal numerical smearing and can also be applied to 3D problems without additional efforts. Recently, Rider and Kothe [31], Gueyffier *et al.* [34], and Harvie and Fletcher [35] proposed schemes to advance the flow front using the geometric and Lagrangian aspects of the VOF transport equation. Also, Harvie and Fletcher [36] used the stream function for updating the flow field.

The objective of present study is to develop a practical numerical algorithm for the analysis of free surface flow problems. Particularly, a study has been performed to improve solution

accuracy associated with the free surface-tracking scheme in the fixed grid system. The free surface-tracking scheme should satisfy the following requirements: (a) it should have a simple structure to be implemented easily in any existing CFD codes, regardless of the solution algorithms of flow field; (b) it should accommodate free surfaces with large deformation on any irregular non-uniform fixed grid systems; (c) it should be applicable to 3D problems without additional efforts. In this study, a new free surface-tracking scheme satisfying these requirements has been proposed. In order to verify the validity of proposed scheme, the broken dam problem and the solitary wave propagation problem have been analysed and the performance of the overall solution procedure was demonstrated. The simulated results obtained by applying the proposed numerical algorithm to the practical 2D and 3D cavity filling and sloshing problems can be found in a separate article [37]. Also, the applicability of the proposed free surface-tracking scheme in an irregular non-uniform mesh has been demonstrated from the simulated results of a simple sloshing problem [33].

2. VOF METHOD

In the VOF method [16], free surface is represented on the fixed grids using fractional fluid volume in a cell (or in a control volume). Each rectangle in Figure 2(c) denotes a unit cell. The fractional volume-of-fluid, f, is defined such that it is equal to unity at any point occupied by the fluid and zero elsewhere. As the free surface moves, the fractional volume-of-fluid of each cell is updated. In a numerical sense, every cell is classified into three categories according to the value of f (see Figure 2(c)). If a cell is completely filled with fluid, the fractional volume-of-fluid of the cell is unity ($f=1$) and the cell is considered to be in the main flow region. If a cell is empty ($f=0$), it belongs to an empty region and its contribution to the computation of flow field is excluded. A cell is considered to be on the free surface when the values of f lies between 0 and 1 ($0<f<1$). A similar concept of 'fractional fluid volume' can be found in the flow analysis network (FAN) method [38, 39]. The FAN-type method basically assumes a quasi-steady Hele–Shaw flow in a thin channel. Movement of free surface is accomplished by calculating net mass fluxes through control surfaces and by updating the fractional fluid volume in each control volume. Application of the FAN-type method can be found in the simulations of injection molding process [40] and resin transfer molding [41].

Hirt and Nichols [16] presented the VOF method by introducing a transport equation of f and by exploiting the donor–acceptor scheme [14]. Discontinuity in f propagates according to the following transport equation:

$$\frac{\partial f}{\partial t}+\mathbf{u}\cdot\nabla f=0 \tag{1}$$

where $\mathbf{u}$ denotes the velocity vector which can be found from solution of the flow field. By solving Equation (1), distribution of f is obtained and thus free surface location can be identified. In a physical sense, Equation (1) implies mass conservation of one phase in the mixture. Numerically, Equation (1) is characterized as a hyperbolic or pure convection equation.

Since the movement of free surface is accomplished by solving Equation (1) in the VOF method, instead of deforming the mesh as in the Lagrangian method or tracing marker particles

as in the MAC method, an overall solution algorithm becomes simple and efficient. Combined with advantages of fixed grids which can accommodate complex geometry, the VOF method is adaptable to any existing CFD codes regardless of the solution methods such as FDM, FVM or FEM. For this reason, the VOF-based methods have been used extensively in the simulation of general free surface flow problems. Several extended or modified versions of the VOF method can be found elsewhere [17–32].

However, the VOF-based method has difficulties in determining a free surface location on the fixed grids. It is well known that the numerical solution of Equation (1) tends to smear. The gradient of f, which should be singular at the moving boundary in physical reality, becomes finite in the numerical solution. This phenomenon is known as a 'false numerical diffusion'. Therefore, the success of the VOF-based methods is strongly dependent on its ability of transporting f through the fixed grids with minimal numerical smearing. In order to suppress the numerical smearing, various schemes have been proposed. Generally, those schemes are categorized into two groups, depending on how the transport equation (Equation (1)) is treated. Some researchers have attempted to solve Equation (1) directly [20, 24–26, 28]. They considered f as another unknown variable and obtained a solution of Equation (1) discretized on a computational mesh. On the other hand, Takewaki *et al.* [42] proposed a cubic-interpolated propagation (CIP) method to solve hyperbolic equations. In the CIP method, which is based on the fact that not only a variable but also its spatial derivative propagates with the velocity, the spatial profile within each grid is interpolated with a cubic polynomial. A unified 2D hyperbolic solver, which can treat solid, liquid and gas simultaneously, was developed and applied to various problems. Recently, Makuuchi *et al.* [43] presented an implicit CIP method in 2D which can overcome the limitation of time step size in the explicit scheme. Other researchers have traced the free surface location using volume flux-based schemes on a staggered mesh in finite volume or finite difference frameworks [16, 17, 19, 21, 23, 29–32, 44–46]. They improved or modified the advection schemes such as the donor–acceptor scheme [14] and the van Leer scheme [47].

3. NEW FREE SURFACE-TRACKING SCHEME

In order to transport f with minimal numerical smearing in the VOF method, a new free surface-tracking algorithm is proposed. In the proposed algorithm, free surface location is traced by calculating fluid volume fluxes on the fixed finite element mesh and by updating the values of f using the donor–acceptor scheme. In the following, discussions are made on how the actual fluid volume flux through the cell boundary can be evaluated by considering both the free surface orientation and the value of f in each cell.

3.1. Wet-out fraction at cell boundary

In order to trace the free surface location on a fixed mesh using a volume flux-based scheme, fluid volume fluxes through every cell boundary should be calculated. When using the VOF method, f is defined for the cell, not on the node. This means that in contrast to the momentum or energy equations, another scheme is required to integrate the transport equation of f (Equation (1)). In the present study, finite elements are treated as cells (or control

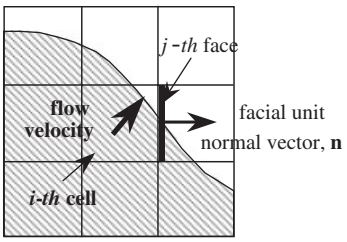

(a)

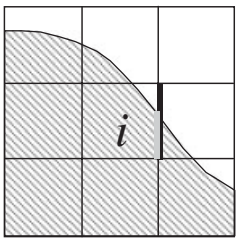

A_J A_J^{wet}

$$f_{\Gamma_j} = \frac{A_J^{wet}}{A_J}$$

(b)

Figure 3. Definitions of (a) cell, face and facial normal vector and (b) wet-out fraction, f_{Γ_j}.

volumes). The transport equation of f written in a conservative form is integrated over each finite element (cell) as follows:

$$\int_V \left[\frac{\partial f}{\partial t} + \mathbf{u} \cdot \nabla f \right] \mathrm{d}V = 0 \tag{2}$$

To handle the time derivative in Equation (2), explicit time integration has been adopted. Generally, implicit integration gives a solution with higher accuracy, but requires more complex and time-consuming algorithm. In the explicit integration, on the other hand, values at the new time step are updated from those at the old time step using the known flow field. In the present study, explicit integration has been adopted for simplicity in updating the free surface location. After the divergence theorem is applied and the time integration is performed, Equation (2) is reduced to

$$f_i^{\text{new}} = f_i^{\text{old}} + \frac{\Delta t}{V_i} \left[-\sum_j (f_{\Gamma_j} \mathbf{u} \cdot \mathbf{n}) A_j \right] \tag{3}$$

where the subscripts i and j represent the cell and the face numbers, respectively. f_i^{new} and f_i^{old} denote the values of f in the ith cell at the new and the old time steps. Δt is the size of time increment, V_i is the volume of the ith cell and A_j is the area of the jth face. $\mathbf{u}$ and $\mathbf{n}$ are the velocity and the unit outward normal vectors at the jth face, respectively (see Figure 3(a)). From Equation (3), it can be stated that the change in fluid volume in a cell during a given time interval is equal to the net fluid volume flux through every cell boundary. Here, f_{Γ_j} represents the 'actual fractional volume-of-fluid' at the jth face of the ith cell during a given time increment [30]. Also, f_{Γ_j} can be interpreted as the wet-out fraction

at a cell boundary, which indicates to what extent the cell boundary is wetted by the fluid (see Figure 3(b)). The basic idea underlying the wet-out fraction is similar to the 'effective flowing time' in the net inflow method [46].

$$f_{\Gamma_j} = \frac{\text{fluid volume transferred through } \Gamma_j}{\text{total volume transferred through } \Gamma_j} \tag{4}$$

In general, f_{Γ_j} in Equation (3) is dependent upon the free surface orientation and the value of f in the cell as well as the size of time increment Δt. However, due to the explicit nature of the time integration adopted in this study, dependency of f_{Γ_j} on Δt becomes out of question. As a result, f_{Γ_j} is a function of the free surface orientation and f_i so that

$$f_{\Gamma_j} = f_{\Gamma_j}(\text{free surface orientation},\ f_i) \tag{5}$$

3.2. *Orientation vector representing free surface configuration*

In order to find free surface configuration in a cell, the status of neighbouring cells should be taken into consideration as stated in Equation (5). In the present study, to avoid considering a large number of cases or introducing complex functional forms as in previous studies [16, 17, 19, 21, 23, 29–32, 44–46], the *orientation vector*, $\mathbf{r}$, is defined in a cell as

$$\mathbf{r} = \frac{\sum_j (f_{ij} \cdot V_{ij})\mathbf{n}_j}{\left|\sum_j (f_{ij} \cdot V_{ij})\mathbf{n}_j\right|} \tag{6}$$

where f_{ij} and V_{ij} represent the fractional volume-of-fluid and the volume of the cell adjacent to the jth face of the ith cell, respectively. $\mathbf{n}_j$ denotes the outward unit vector normal to the jth face, Γ_j.

As can be seen in Equation (6), orientation vector is obtained by considering how the values of f in the neighbouring cells are distributed. The orientation vector was made to be unity in magnitude through normalization and was designed to indicate the direction where fluid is abundant (see Figure 4(a)). The free surface configuration in a cell is then assumed to be perpendicular to the orientation vector. From the definition, the orientation vector is affected by the characteristics of the grid system (through V_{ij} and $\mathbf{n}_j$ in Equation (6)). When a regular grid system of uniform mesh is used, orientation vectors can produce exact free surface configuration within the accuracy in the solution of f field. Even in a non-uniform grid system, they can give approximate configuration of free surface as long as the mesh does not have extremely large aspect ratio. In most of the practical numerical computations, non-uniform grid systems have little influence on the evaluation of orientation vector since the grids are generated in such a way that they are not severely distorted. In the present study, however, in order to take into account a possible influence of various aspect ratios in any arbitrary non-uniform grid system, Equation (6) is modified as

$$\mathbf{r} = \frac{\sum_j (f_{ij} \cdot V_{ij})a_j\mathbf{n}_j}{\left|\sum_j (f_{ij} \cdot V_{ij})a_j\mathbf{n}_j\right|} \tag{7}$$

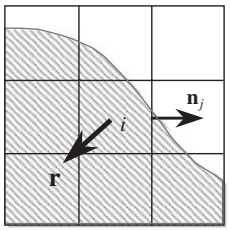

(a)

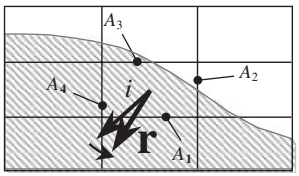

$$a_j = \frac{A_j}{\sum_j A_j}$$

(b)

Figure 4. Definition of orientation vector, **r**.

where a_j denotes the ratio of the jth facial area to the total facial area of the ith cell. Thus, a_j satisfies $\sum_j a_j = 1$. Here, a_j can be considered as a weighting factor used to take non-uniformity of aspect ratios into consideration. In other words, a_j accounts for a tendency that when two neighbouring cells have the same value of f, the actual free surface configuration in a cell becomes parallel with a face of larger facial area (see Figure 4(b)).

When the jth face is a solid wall, there exists no neighbouring cell to refer to in that direction. In such a case, a virtual cell is assumed to exist across the solid wall. The virtual cell is then supposed to have a specific value of f so that the distribution of f can take a linear variation in a local region adjacent to the solid wall. This is expressed as

$$f_{ij(\,j\,=\,\text{solid wall})} = \min[\max(f_i + \Delta f, 0), 1] \tag{8}$$

where Δf denotes the difference in values of f in the ith cell and in the cell opposite to the solid wall. Symmetric planes can be handled in a similar manner.

From the orientation vector, information on the orientation (i.e. slope) of free surface in a cell can be obtained. Therefore, it can be assumed that the free surface in a cell is a straight line in 2D or a plane in 3D which is normal to the orientation vector. In the proposed scheme, the slope of free surface in a cell is first obtained and the location of free surface represented by a straight line (in 2D) or a plane (in 3D) is then adjusted according to the value of f of the cell. Hence, the proposed free surface-tracking scheme can be classified as a sort of PLIC (piecewise linear interface calculation) method [23, 29–31, 45] in contrast to SLIC (simple line interface calculation) method [44]. However, the common difficulty encountered in such volume flux-based schemes lies in the determination of fluid volume flux at the cell boundary. For that matter, the baby-cell method utilizing a linear mapping in the finite element method is proposed (Section 3.3). Orientation vector is not used to simply represent the free surface as a straight line (in 2D) or a plane (in 3D) locally, but utilized as a reference for the determination of fluid volume flux at the cell boundary (Section 3.3). In addition, from an algorithmic standpoint for embodiment of the basic idea, the baby-cell

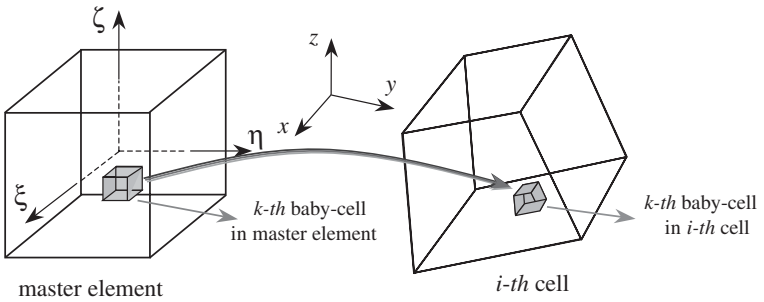

Figure 5. Definition of baby-cell.

method preserves a simple structure consistently in 2D and 3D, while previous PLIC methods resort to complicated algorithms even in 2D and the extension to 3D requires a much more complicated algorithmic structure.

3.3. Baby-cells representing uniform sub-volumes

Now that free surface configuration in a cell has been found from the orientation vector, actual fluid volume fluxes at the cell boundaries can be determined with reference to the value of f in the cell. However, even for the same free surface configuration, there may exist a great number of different cases according to the values of f. The actual fluid volume flux through each cell boundary should be determined depending on which face of the cell and how much of that face is wetted by the fluid, rather than how much of the cell is filled with the fluid (i.e. the value of f). In this study, baby-cells are utilized for this purpose. The baby-cells are defined in a master element (of FEM) in such a way that they can divide the volume of the master element into uniform sub-volumes with equal volumetric contribution (see Figure 5). Corresponding baby-cells in a physical element can be obtained using a linear mapping between the master and the physical elements. The name of *baby-cell* implies that one baby-cell in the master element has the one and only counterpart in every physical element. If the physical element is distorted, corresponding baby-cells become also distorted, but still have equal volumetric contribution (i.e. they still represent uniform sub-volumes). This is because the determinant of the Jacobian matrix in the linear transformation is constant over one physical element. Linearity of the transformation adopted in the present finite element formulation makes this process possible.

The baby-cell method proposed in this study is based on the use of an arbitrary irregular non-uniform fixed mesh composed of quadrilateral elements in 2D and hexahedral elements in 3D. Therefore, while baby-cells in the master element have a shape of a regular square in 2D or a regular hexahedron in 3D, those in a physical element of the arbitrary irregular non-uniform mesh have a shape of a general quadrangle in 2D or a general hexahedron in 3D, following the shape of the physical element. The baby-cells are utilized to determine the wet-out fraction at each cell boundary in the following manner:

(1) A plane, which is normal to the orientation vector, **r**, and passes through the centroid of a cell, is assumed (see Figure 6(a)). The plane does not have to pass through

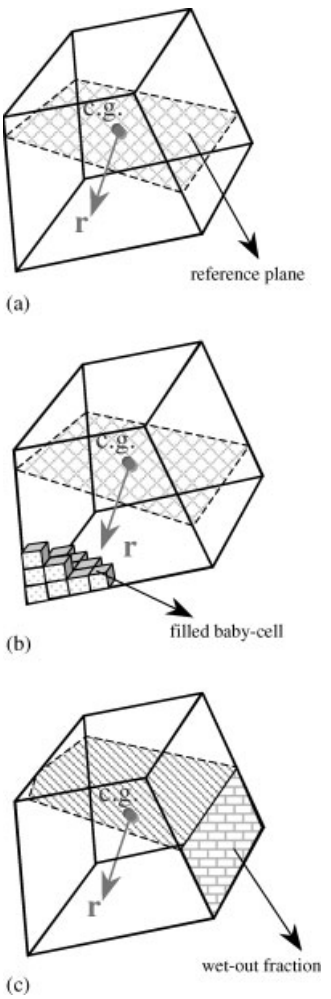

Figure 6. Schematic illustration of the procedure for evaluating wet-out fraction at the cell boundary: (a) Construct a reference plane normal to the orientation vector, **r**; (b) fill baby-cells sequentially and (c) estimate the accumulated contribution from the filled baby-cells to each cell boundary.

the centroid necessarily because it is used as only a reference plane. That is, the plane plays a single role of determining the relative distance of each baby-cell from itself.

(2) Baby-cells are assumed to be filled up in sequence beginning with the farthest one from the reference plane in the positive direction of orientation vector until fractional fluid volume of the cell reaches its value of f (see Figure 6(b)).

(3) Contributions of the filled baby-cell to each cell boundary are estimated. Consequently, the accumulated contribution from all the filled baby-cells gives wet-out fraction at each cell boundary (see Figure 6(c)).

Following the above procedure, the actual fluid volume flux through each cell boundary can be evaluated. Proposed scheme can trace the moving free surface with minimal numerical smearing because it is based on the physical observation. Furthermore, the proposed scheme needs almost no extra computer storage because baby-cells are created utilizing the existing transformation in FEM. Also, the proposed scheme imposes little amount of burden on computation time as the above procedure is carried out only on the free surface cells. This free surface-tracking procedure took 10% or less of the total computation time. In the present study, the number of baby-cells was chosen as 1600 ($=40\times40$) in 2D and 1000 ($=10\times10\times10$) in 3D. A larger number of baby-cells can yield higher resolution in the estimation of wet-out fraction. In the present calculation, however, the use of a much larger number of baby-cells did not make a big difference in the overall solution accuracy. From definition, the number of baby-cells can affect the accuracy in the calculation of wet-out fractions at the cell boundaries. Although the effects of the number of baby-cells on the accuracy of solution were not investigated in this study, simple consideration shows that the maximum error in the estimated wet-out fraction is 2.5% ($=1/40$) for 1600 baby-cells in 2D and 1% ($=1/10\times10$) for 1000 baby-cells in 3D.

4. GOVERNING EQUATIONS AND FINITE ELEMENT FORMULATION

Governing equations and the boundary conditions for the flow field are described in this section. Finite element formulation to solve the equations is also given.

4.1. Governing equations and boundary conditions

Following assumptions are made for the computation of the flow field:

(1) Moving free surface exists between two immiscible fluids.
(2) Flow is incompressible, viscous and laminar.
(3) Fluids have constant properties.

Governing equations are the continuity equation and the unsteady Navier–Stokes equations for laminar flow of incompressible Newtonian fluids.

$$u_{i,i}=0 \tag{9}$$

$$\frac{\partial u_i}{\partial t}+u_j u_{i,j}=-\frac{1}{\bar{\rho}}\,p_{,i}+\sigma_{ij,j}+S_i \tag{10}$$

where $\sigma_{ij}=\bar{\nu}(u_{i,j}+u_{j,i})$. Here, $\bar{\rho}$ and $\bar{\nu}$ represent the density and the kinematic viscosity, respectively. $\bar{\rho}$ and $\bar{\nu}$ for the free surface cells ($0<f<1$) are obtained using the rule of mixture.

To complete the problem description, an appropriate set of boundary conditions should be specified. In general, the essential boundary condition is given as

$$u_i=b_i \quad \text{on } \Gamma_1 \tag{11}$$

The natural boundary condition can be written as

$$\left[-\frac{1}{\bar{\rho}}\, p\delta_{ij} + \sigma_{ij}\right] n_j = t_i \quad \text{on } \Gamma_2 \tag{12}$$

Here, Γ_1 and Γ_2 are two non-overlapping subsets of the piecewise smooth domain boundary Γ. b_i is the velocity vector prescribed on Γ_1 and t_i is the traction vector prescribed on Γ_2. n_j is the unit outward vector normal to Γ_2.

Initial condition for Equation (10) is given by specifying a velocity field, which satisfies Equation (9) at the initial state.

$$\mathbf{u}(\mathbf{x}, 0) = \mathbf{u}_0(\mathbf{x}) \quad \text{with } \nabla \cdot \mathbf{u}_0 = 0 \tag{13}$$

On the solid wall, no-slip or frictionless boundary conditions can be given. In many cases, frictionless boundaries can be assumed between the fluid and the wall (e.g. References [3, 4, 9, 15, 19, 32]). Impermeable boundary is also assumed at the wall. Therefore, frictionless boundary condition on the solid wall can be expressed as

$$u_i n_i = 0 \quad \text{and} \quad \left[-\frac{1}{\bar{\rho}}\, p\delta_{ij} + \sigma_{ij}\right] s_j = 0 \tag{14}$$

Here, s_j denotes the vector tangential to the solid wall boundary.

While the boundary conditions on the solid wall are straightforward, those on the free surface should be imposed carefully. In the present study, second fluid is kept at the atmospheric pressure, which is taken to be zero. It is also assumed that the stress normal to the free surface is equal to any externally applied normal stress and the stress tangential to the free surface is zero. If surface tension is neglected, above assumptions lead to the following traction-free condition.

$$\left[-\frac{1}{\bar{\rho}}\, p\delta_{ij} + \sigma_{ij}\right] n_j = 0 \tag{15}$$

4.2. Finite element formulation and fractional step method

The spatial domain is discretized with four-node isoparametric quadrilateral elements in 2D and eight-node isoparametric hexahedral elements in 3D. Velocity is represented by bilinear or trilinear polynomials in an element and is defined at all vertices of each element. Pressure is piecewise constant within an element and is defined at the centroid of each element. Equations (9) and (10) are discretized using the Galerkin approximation. Semi-discretized equation for $\mathbf{u}$, which is an ordinary differential equation (ODE) in time, is obtained as

$$\mathbf{M}\dot{\mathbf{u}} + \mathbf{C}(\mathbf{u})\mathbf{u} + \mathbf{K}\mathbf{u} - \mathbf{H}\mathbf{p} - \mathbf{F} = \mathbf{0} \tag{16}$$

For detailed definition of matrices, see, for example, Reference [48].

The continuity equation (Equation (9)) is discretized on the basis of element as follows [15]:

$$\mathbf{h}_e^{\mathrm{T}}\mathbf{u}_e = 0 \quad (e = 1, 2, 3, \ldots, \mathrm{NE}) \tag{17}$$

Here, NE denotes the total number of finite elements participating in the computation.

In the present study, Equation (16) was integrated in time using the explicit fractional time-stepping method [15]. Fractional step method has been originally proposed by Chorin [49] in the finite difference framework. In this method, the pressure gradient term is decoupled from those of convection, diffusion and other external forces. In this procedure, the intermediate velocity does not necessarily satisfy the continuity constraint. Thus, the end-of-step velocity is obtained by adding the dynamic effect of unknown pressure to the intermediate velocity. That is, at the next step, the pressure is obtained from the continuity constraint and the velocity is corrected [15, 49–53]. In the explicit element-by-element fractional step method [15], the intermediate velocity is obtained by integrating Equation (16) explicitly. The velocity correction is then made by adjusting the pressure of each element in such a way that local divergence of the velocity in the element vanishes. For a detailed procedure, one can refer to Reference [15].

Another important point in the formulation of Navier–Stokes equations is that the numerical algorithm should be able to resolve the convection-dominated nature of the flow. Scalar quantities in the incompressible flow field are transported along the streamline when the diffusion effect is negligible compared to the convection. Based on this idea, the anisotropic balancing diffusion method [54] and the consistent streamline upwind/Petrov–Galerkin (SUPG) method [55] have been proposed. In the present study, the consistent SUPG method has been adopted to deal with the convection dominated flow.

5. SOLUTION PROCEDURE

Using the free surface-tracking scheme and the solution method of Navier–Stokes equations described in the previous sections, the solution procedure can be summarized as follows (see Figure 7)

(1) Define the problem. For a given geometry
   - specify material properties and parameters;
   - generate a mesh system;
   - obtain information on mesh topology;
   - specify boundary and initial conditions.

(2) Identify the computational domain. The cells which have f values greater than 0.5 are supposed to comprise the computational domain [19]. In the following step, specify the velocity on the new computational domain. Newly included domain has nodes at which velocity is not yet determined and remains zero (Equation (20)).

(3) For the given free surface configuration, obtain velocity and pressure fields at the new time step.

(4) With the new flow field, update the location of the free surface:
   - obtain orientation vectors on every free surface cell;
   - estimate the wet-out fractions at every cell boundary;
   - determine the size of the time increment (Equation (19));
   - advance the free surface.

(5) Repeat steps (2)–(4) until the prescribed final time is reached.

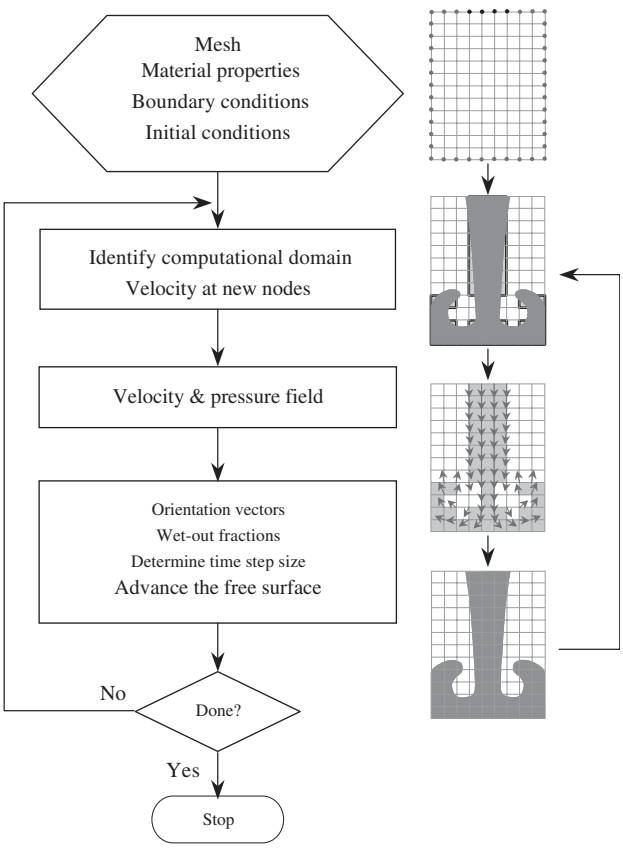

Figure 7. Solution procedure for the fluid flow with moving free surface.

In this study, emphasis is placed on the new free surface-tracking scheme that can trace the free surface with minimal numerical smearing. The proposed free surface-tracking scheme became much more efficient when combined with the fractional step method in the solution of Navier–Stokes equations. In addition to the explicit time integration methods adopted in the momentum equations and the transport equation of f, the diagonal lumped mass matrix representation was introduced to improve both speed and efficiency of overall solution algorithm. The consistent mass matrix $\mathbf{M}$ was replaced with a diagonal mass matrix using a standard row-sum technique [50].

5.1. Size of time increment and stability consideration

Though the explicit time integration methods adopted in the momentum equations as well as in the transport equation of f are simple and fast, the solution procedure may become unstable when the size of time increment becomes too large. However, it has been reported that the explicit time integration method in combination with the diagonal lumped mass matrix representation showed a good performance in general [50]. Also, it should be kept in mind

that even though the implicit time integration methods do not suffer from stability restriction, they do not always guarantee good accuracy at a large Courant number. In the explicit method, stability limit of the time step size is given by the following restriction in the CFL number

$$\mathrm{CFL} = \left(\frac{|u|}{\Delta x} + \frac{|v|}{\Delta y} + \frac{|w|}{\Delta z} \right) \Delta t \leqslant 1 \tag{18}$$

The size of time increment in the VOF method should be determined so that the fluid cannot be transported through more than one cell during a single time increment [16]. In this study, the fluid volume fluxes through cell boundaries are estimated first. The size of time increment is then determined in such a way that the net incoming fluid volume should not exceed the empty volume of a cell and the net outgoing fluid volume should not exceed the present fluid volume in a cell during a single time step Δt [32].

For a cell with positive net volume flux:

$$\Delta t \leqslant \frac{(1 - f_i)V_i}{[-\sum_j (f_{\Gamma_j} \mathbf{u} \cdot \mathbf{n}) A_j]} \tag{19a}$$

For a cell with negative net volume flux:

$$\Delta t \leqslant \frac{(0 - f_i)V_i}{[-\sum_j (f_{\Gamma_j} \mathbf{u} \cdot \mathbf{n}) A_j]} \tag{19b}$$

The smallest time increment from the above equations is chosen so that the criterion is satisfied simultaneously in all the cells within the computational domain. Accordingly, Equation (18) is satisfied automatically.

5.2. *Velocity specification at new nodes*

When we proceed to the next computational time step, a region may exist which is excluded from or included into the computational domain due to retreat or advance of the free surface. In particular, the newly included region often has nodes at which velocity is not yet determined and remains zero. Therefore, a procedure assigning reasonable values of velocity to such new nodes is needed. In the present study, velocity at the newly added node is obtained from the average velocities of neighbouring cells through the volume-weighted averaging [15] (see Figure 8),

$$u^{\text{new node}} = \frac{\sum \bar{\mathbf{u}}_e \cdot V_\mathrm{e}}{\sum V_\mathrm{e}} \tag{20}$$

where $\mathbf{u}^{\text{new node}}$ represents the velocity at the new node. $\bar{\mathbf{u}}_e$ and V_e represent the average velocity and the volume of neighbouring cell, respectively.

6. VERIFICATION OF NUMERICAL SCHEME

In order to verify the validity of the proposed scheme, broken dam problem and solitary wave propagation problem have been analysed. Numerical examples tested in this study

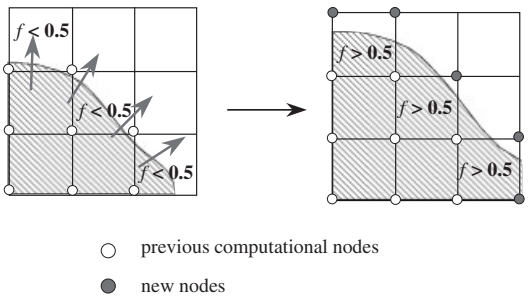

Figure 8. New nodes entering the computational domain.

have been challenged through various experimental, numerical and analytical approaches. For the broken dam problem, experimental data [56] as well as numerically simulated results [5, 8–10, 15, 16, 19, 32, 46] are available, while for solitary wave propagation problem, experimental data [57], numerical results [7, 9, 11] and analytical solution [58, 59] can be found. On the other hand, simulated results of practical 3D flow problems with large free surface deformation (e.g. cavity filling problems and sloshing problems) obtained with the proposed numerical scheme can be found in separate articles [33, 37].

6.1. Broken dam problem

As a first example, the broken dam problem is considered. This problem is selected because the initial flow configuration is simple and the experimental data are available as well [56]. Since both advance and retreat of the free surface exist, this problem enables one to test the free surface-tracking technique more thoroughly. Therefore, many numerical works have been performed for the problem [5, 8–10, 15, 16, 19, 32, 46].

The definition of the problem is illustrated in Figure 9. A rectangular column of water in hydrostatic equilibrium is confined between a vertical wall and the gate. The gate is suddenly removed at time $t = 0^+$ and the water column starts to collapse under the influence of gravity, forming an advancing water wave to the right. An initial flow configuration was chosen as a square column ($H \times H$, $H = 0.05175\,\mathrm{m}$), following the experimental condition by Martin and Moyce [56]. Boundary conditions are shown in Figure 9. Frictionless boundary conditions are specified on the bottom and the vertical walls. Density and viscosity of water are taken as $1000\,\mathrm{kg/m^3}$ and 1×10^{-3} Pa.s, respectively. The ambient fluid is air. Density is $1\,\mathrm{kg/m^3}$ and viscosity is 1×10^{-5} Pa.s. The gravitational acceleration is $g = 9.8\,\mathrm{m/s^2}$. To investigate the influence of grid system on the simulated results, four meshes of different grid density have been used; three uniform meshes ($31 \times 13, 49 \times 20, 61 \times 25$) and a non-uniform mesh (49×20, see Figure 10).

Free surface profiles and corresponding pressure contours obtained with the non-uniform 49×20 mesh are shown in Figure 11. The water column starts to collapse from the upper right. The water wave then accelerates rapidly along the floor in the right direction as time elapses. In Figure 12, the position of water wave front and the height of residual water column are plotted as functions of elapsed time, and compared with the experimental data [56]. For convenience, dimensionless time and length are defined as $t^* = t\sqrt{(g/H)}$ and $x^* = x/H$, respectively. All the

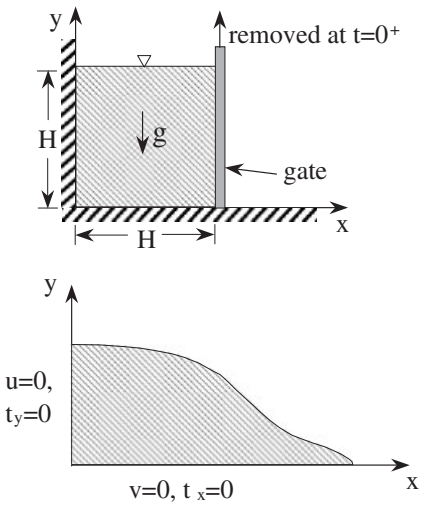

Figure 9. Broken dam problem.

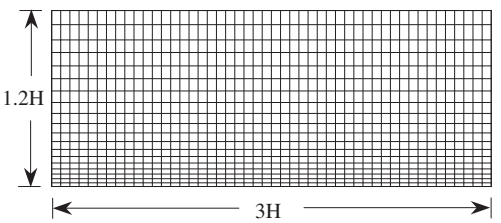

Figure 10. Non-uniform 49×20 mesh used for the broken dam problem.

results obtained with four different meshes show good agreement, with a slight deviation in the result obtained with a uniform 31×13 mesh, which has the smallest number of nodes in the present calculation. Good agreement with the experimental data indicates that the present numerical scheme is capable of predicting the collapse of water column accurately.

6.2. Solitary wave propagation

As a second example, propagation of a solitary wave is analysed. Solitary wave is defined as a single wave elevated above the surrounding undisturbed water level, travelling only in the direction of wave propagation with a constant velocity throughout the observable time interval. Laitone [58] and Byatt-Smith [59] obtained an analytic solution for the inviscid surface wave in the infinitely long channel. Maxworthy [57] carried out experiments on the interaction of single wave with vertical wall. Numerical studies have been also performed using various approaches. The MAC method was used by Chan and Street [11] and the ALE method was employed by Ramaswamy and Kawahara [7] and Choi [9].

Definition of the problem is shown in Figure 13. The fluid is water and the ambient is air. Properties of water and air are identical as in the broken dam problem. Analytic solutions are

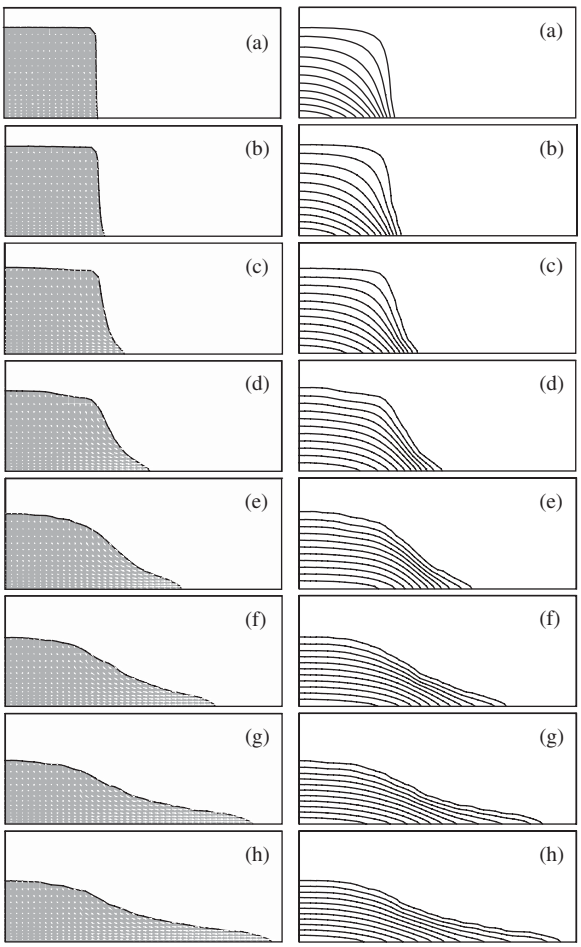

Figure 11. Free surface profiles (left) and pressure contours (right) for the broken dam problem. (a) 0.01 s, (b) 0.02 s, (c) 0.04 s, (d) 0.06 s, (e) 0.08 s, (f) 0.10 s, (g) 0.12 s and (h) 0.13 s.

obtained for an infinitely long channel, while computation should be done in a finite domain. Fluid at a distance from the wave crest is essentially still. Therefore, the flow domain is taken so that the dimension in the direction of wave propagation is sufficiently large compared to the wave height. Referring to [7], depth of still water and horizontal length between two vertical walls are taken as $d = 1$ (m) and $L = 16$ (m), respectively. Boundary and initial conditions are shown in Figure 14. Frictionless boundary conditions were specified on the bottom and the vertical walls. For comparison, initial conditions were given following the Laitone's approximation of the solitary wave [58].

Calculations were carried out for $H/d = 0.20$, 0.25, 0.30, 0.35, 0.40, 0.45, 0.50 and 0.55. The mesh used for $H/d = 0.40$ consists of non-uniform 81×37 grids (see Figure 15). For $H/d = 0.40$, velocity vectors and pressure contours at the initial stage are shown in Figures 16(a) and 17(a), respectively. The calculated wave profiles and corresponding velocity vector

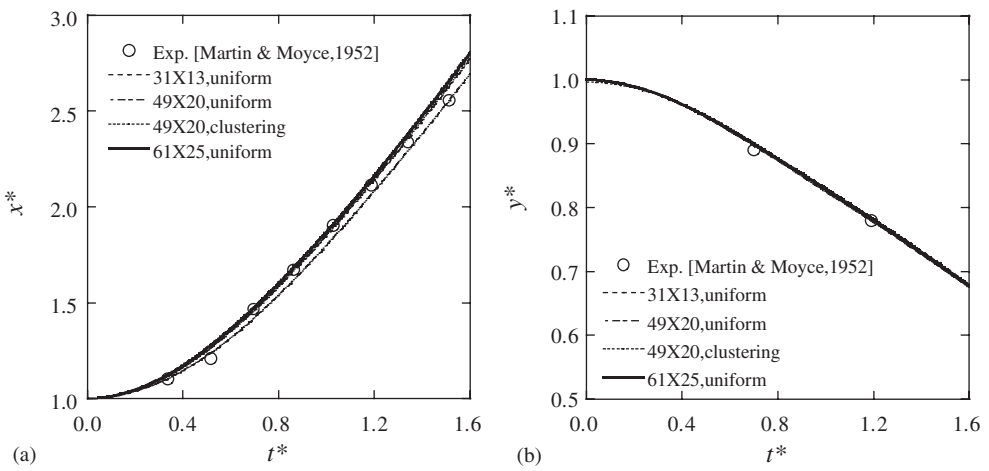

Figure 12. (a) The position of the water wave front and (b) the height of the residual water column as functions of time. Comparison of the numerical results using four different grids with the experimental data [56].

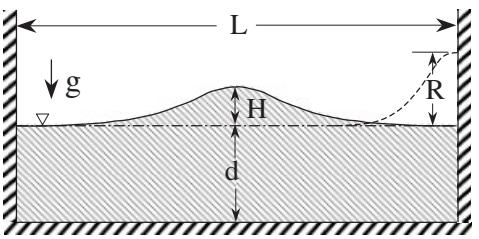

Figure 13. Propagation of a solitary wave.

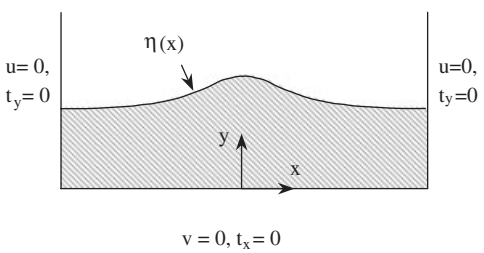

Figure 14. Boundary and initial conditions for the solitary wave propagation problem.

fields are shown in Figure 16, while the pressure contours are shown in Figure 17. The initial kinetic energy is converted into potential energy at the vertical wall as shown in Figures 16(c) or 16(g). Pressure remains almost hydrostatic and this agrees well with the Laitone's analytic solution [58]. Maximum run-up of the solitary wave against the vertical wall is shown in Figure 18 for various incident wave heights. The maximum run-up attained by the wave

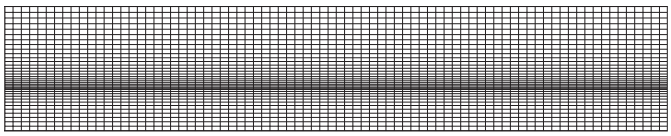

Figure 15. Non-uniform 81×37 mesh used for the solitary wave propagation problem.

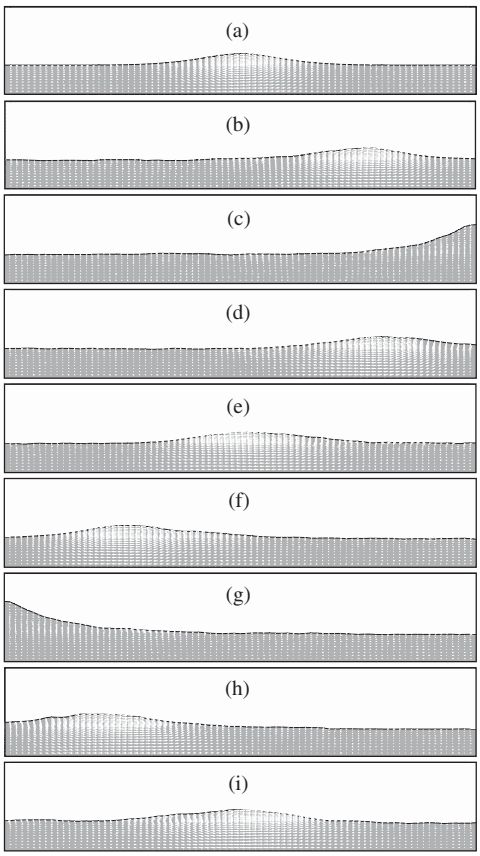

Figure 16. Wave profiles and velocity vectors for the solitary wave propagation problem. (a) 0 s, (b) 1.2 s, (c) 2.3 s, (d) 3.4 s, (e) 4.6 s, (f) 5.7 s, (g) 6.9 s, (h) 8.1 s and (i) 9.3 s.

is always greater than twice the initial wave height. Byatt-Smith [59] obtained an explicit expression for the maximum run-up $R_{\max}/d$ of a solitary wave of initial wave height H/d,

$$\frac{R_{\max}}{d} = 2\left(\frac{H}{d}\right) + \frac{1}{2}\left(\frac{H}{d}\right)^2 + O\left[\left(\frac{H}{d}\right)^3\right] \tag{21}$$

In Figure 18, the present results show good agreement with other numerical and experimental results. It is clearly seen that there exists no numerically induced damping effect. Compared

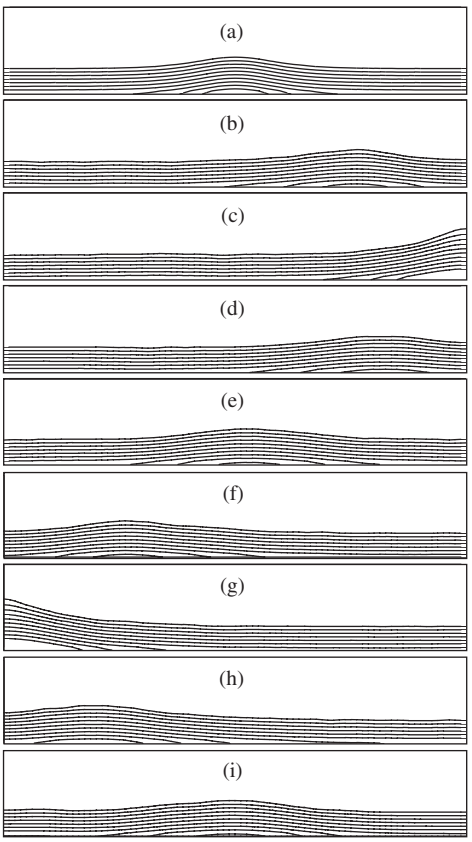

Figure 17. Pressure contours for the solitary wave propagation problem. (a) 0 s, (b) 1.2 s, (c) 2.3 s, (d) 3.4 s, (e) 4.6 s, (f) 5.7 s, (g) 6.9 s, (h) 8.1 s and (i) 9.3 s.

with the analytic solution, a negative spatial phase shift is observed in the computed results. This spatial phase shift is attributable to the finite time of interaction at the vertical wall. In Figure 19, the magnitude of spatial phase shift for $H/d = 0.40$ is $\Delta X/d \approx -1.3$ and this agrees favorably with the experimental observation [57].

7. CONCLUDING REMARKS

A new VOF-based algorithm has been proposed for the simulation of transient free surface flow problems. The new free surface-tracking scheme is characterized by the orientation vector and the baby-cell. Orientation vector gives information on the free surface orientation in a cell by inspecting the distribution of f in the vicinity. In order to trace the free surface on a fixed mesh using the volume flux-based scheme, the actual fluid volume flux through cell boundary should be evaluated. For that purpose, the baby-cell was devised to represent uniform sub-volume at the designated position in a cell. Without introducing additional

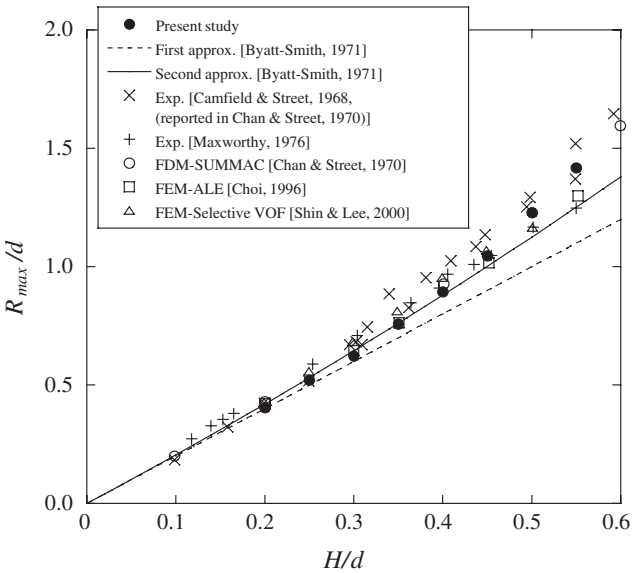

Figure 18. Maximum run-up height of the solitary wave against the vertical wall for various incident wave heights. Comparison of the present numerical results with previous works.

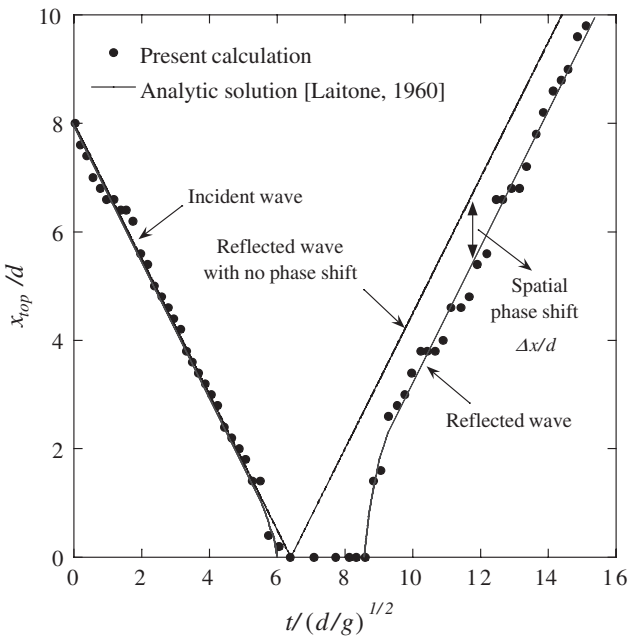

Figure 19. Spatial phase shift of the wave crest for $H/d = 0.4$. Comparison of the present numerical results with the analytic solution [58].

functional expressions, baby-cells were constructed by utilizing a mapping characteristic in FEM. With orientation vector and baby-cell, free surface could be traced with minimal numerical smearing. Validity of the proposed free surface-tracking scheme has been shown from simulation of broken dam and solitary wave propagation problems. The simulated results have also demonstrated excellent performance of overall solution algorithm. Furthermore, with a relatively simple structure, the proposed scheme can be easily implemented in 3D problems.

NOMENCLATURE

A_j	area of the jth face
a_j	ratio of the jth facial area to the total facial area
b_i	velocity boundary condition
$\mathbf{C}(\mathbf{u})$	convection matrix
$\mathbf{F}$	force matrix
f	fractional volume-of-fluid of cell
f_{Γ_j}	wet-out fraction at the jth face
$\mathbf{H}$	pressure gradient matrix
$\mathbf{h}_e$	element pressure gradient matrix
$\mathbf{K}$	diffusion matrix
$\mathbf{M}$	consistent mass matrix
$\mathbf{n}$	unit outward normal vector
p	pressure
$\mathbf{r}$	orientation vector
S_i	external force vector
t	time
Δt	time increment
t_i	traction boundary condition
$\mathbf{u}$	velocity vector
u, v, w	velocity components
V_i	volume of the ith cell

Greek letters

Γ_j	the jth cell boundary
$\bar{\nu}$	coefficient of kinematic viscosity
$\bar{\rho}$	density
σ_{ij}	viscous stress tensor

Subscripts

e	element
i	cell number
j	face number

ACKNOWLEDGEMENTS

This work was supported by the Brain Korea-21 project and by Korea Ministry of Science and Technology through the National Lab Project.

REFERENCES

1. Floryan JM, Rasmussen H. Numerical methods for viscous flows with moving boundaries. *Applied Mechanics Reviews* 1989; **42**:323–341.
2. Hirt CW, Cook JL, Butler TD. A Lagrangian method for calculating the dynamics of an incompressible fluid with free surface. *Journal of Computational Physics* 1970; **5**:103–124.
3. Ramaswamy B, Kawahara M, Nakayama T. Lagrangian finite element method for the analysis of two-dimensional sloshing problems. *International Journal for Numerical Methods in Fluids* 1986; **6**:659–670.
4. Okamoto T, Kawahara M. Two-dimensional sloshing analysis by Lagrangian finite element method. *International Journal for Numerical Methods in Fluids* 1990; **11**:453–477.
5. Kim MS, Lee WI, Lee JS. Analysis of the mold filling process with phase change considering the non-steady effect. *International Polymer Processing* 1996; **11**:58–67.
6. Hirt CW, Amsden AA, Cook JL. An arbitrary Lagrangian–Eulerian computing method for all flow speeds. *Journal of Computational Physics* 1974; **14**:227–253.
7. Ramaswamy B, Kawahara M. Arbitrary Lagrangian–Eulerian finite element method for unsteady, convective, incompressible viscous free surface fluid flow. *International Journal for Numerical Methods in Fluids* 1987; **7**:1053–1075.
8. Huerta A, Liu WK. Viscous flow with large free surface motion. *Computer Methods in Applied Mechanics and Engineering* 1988; **69**:277–324.
9. Sung J, Choi HG., Yoo JY. Finite element simulation of thin liquid film flow and heat transfer including a hydraulic jump. *International Journal for Numerical Methods in Engineering* 1999; **46**:83–101.
10. Harlow FH, Welch JE. Numerical calculation of time-dependent viscous incompressible flow of fluid with free surface. *Physics of Fluids* 1965; **8**:2182–2189.
11. Chan RKC, Street RL. A computer study of finite-amplitude water waves. *Journal of Computational Physics* 1970; **6**:68–94.
12. Amsden AA, Harlow FH. The SMAC method: a numerical technique for calculating incompressible fluid flow. *Los Alamos Scientific Laboratory Report*, LA-4370. 1970.
13. Hirt CW, Cook JL. Calculating three-dimensional flows around structures and over rough terrain. *Journal of Computational Physics* 1972; **10**:324–340.
14. Ramshaw JD, Trapp JA. A numerical technique for low-speed homogeneous two-phase flow with sharp interface. *Journal of Computational Physics* 1976; **21**:438–453.
15. Nakayama T, Mori M. An Eulerian finite element method for time-dependent free surface problems in hydrodynamics. *International Journal for Numerical Methods in Fluids* 1996; **22**:175–194.
16. Hirt CW, Nichols BD. Volume of fluid (VOF) method for the dynamics of free boundaries. *Journal of Computational Physics* 1981; **39**:201–225.
17. Nichols BD, Hirt CW, Hotchkiss RS. SOLA-VOF: a solution algorithm for transient fluid flow with multiple free boundaries. *Los Alamos Scientific Laboratory Report*, LA-8355. 1980.
18. Partom IS. Application of the VOF method to the sloshing of a fluid in a partially filled cylindrical container. *International Journal for Numerical Methods in Fluids* 1987; **7**:535–550.
19. Jun L, Spalding DB. Numerical simulation of flows with moving interfaces. *PhysicoChemical Hydrodynamics* 1988; **10**:625–637.
20. Dhatt G, Gao DM, Cheikh AB. A finite element simulation of metal flow in moulds. *International Journal for Numerical Methods in Engineering* 1990; **30**:821–831.
21. Chan KS, Pericleous K, Cross M. Numerical simulation of flows encountered during mold-filling. *Applied Mathematical Modelling* 1991; **15**:624–631.
22. Minaie B, Stelson KA, Voller VR. Analysis of flow patterns and solidification phenomena in the die casting process. *Journal of Engineering and Materials Technology* 1991; **113**:296–302.
23. Ashgriz N, Poo JY. *FLAIR*: Flux line-segment model for advection and interface reconstruction. *Journal of Computational Physics* 1991; **93**:449–468.
24. Usmani AS, Cross JT, Lewis RW. A finite element model for the simulations of mould filling in metal casting and the associated heat transfer. *International Journal for Numerical Methods in Engineering* 1992; **35**: 787–806.
25. Rice AB. Numerical simulation of mold filling processes. *Ph.D. Thesis*, Purdue University, 1993.
26. Swaminathan CR, Voller VR. A time-implicit filling algorithm. *Applied Mathematical Modelling* 1994; **18**: 101–108.

27. Kothe DB, Mjolsness RC, Torrey MD. RIPPLE: a computer program for incompressible flows with free surfaces. *Los Alamos National Laboratory Report*, LA-12007-MS. 1994.
28. Lewis RW, Usmani AS, Cross JT. Efficient mould filling simulation in castings by an explicit finite element method. *International Journal for Numerical Methods in Fluids* 1995; **20**:493–506.
29. Mashayek F, Ashgriz N. A hybrid finite-element-volume-of-fluid method for simulating free surface flows and interfaces. *International Journal for Numerical Methods in Fluids* 1995; **20**:1363–1380.
30. Rudman M. Volume-tracking methods for interfacial flow calculations. *International Journal for Numerical Methods in Fluids* 1997; **24**:671–691.
31. Rider WJ, Kothe DB. Reconstructing volume tracking. *Journal of Computational Physics* 1998; **141**:112–152.
32. Shin S, Lee WI. Finite element analysis of incompressible viscous flow with moving free surface by selective volume of fluid method. *International Journal of Heat and Fluid Flow* 2000; **21**:197–206.
33. Kim MS. Finite element study of fluid flow with moving free surface. *Ph.D. Thesis*, Seoul National University, 1998.
34. Gueyffier D, Li J, Nadim A, Scardovelli R, Zaleski S. Volume-of-fluid interface tracking with smoothed surface stress methods for three-dimensional flows. *Journal of Computational Physics* 1999; **152**:423–456.
35. Harvie DJE, Fletcher DF. A new volume of fluid advection algorithm: the stream scheme. *Journal of Computational Physics* 2000; **162**:1–32.
36. Harvie DJE, Fletcher DF. A new volume of fluid advection algorithm: the defined donating region scheme. *International Journal for Numerical Methods in Fluids* 2001; **35**:151–172.
37. Kim MS, Park JS, Lee WI. A new VOF-based numerical scheme for the simulation of fluid flow with free surface. Part II: Application to the cavity filling and sloshing problems. *International Journal for Numerical Methods in Fluids* 2003; **42**:791–812.
38. Tadmor Z, Broyer E, Gutfinger C. Flow analysis network (FAN)—a method for solving flow problems in polymer processing. *Polymer Engineering Science* 1974; **14**:660–665.
39. Broyer E, Gutfinger C, Tadmor Z. A theoretical model for the cavity filling process in injection molding. *Transactions of Society of Rheology* 1975; **19**:423–444.
40. Hieber CA, Shen SF. A finite-element/finite-difference simulation of the injection-molding filling process. *Journal of Non-Newtonian Fluid Mechanics* 1980; **7**:1–32.
41. Kang MK, Lee WI, Yoo JY, Cho SM. Simulation of mold filling process during resin transfer molding. *Journal of Materials Processing & Manufacturing Science* 1995; **3**:297–313.
42. Takewaki H, Nishiguchi A, Yabe T. Cubic interpolated pseudo-particle method (CIP) for solving hyperbolic-type equations. *Journal of Computational Physics* 1985; **61**:261–268.
43. Makuuchi H, Aoki T, Yabe T. Implicit CIP (cubic-interpolated propagation) method in two dimensions. *JSME International Journal*, *Series B* 1997; **40**:365–376.
44. Noh WF, Woodward P. SLIC (simple line interface calculation). In *Proceedings of the 5th International Conference on Numerical Methods in Fluid Dynamics*, Lecture Notes in Physics, van de Vooren AI, Zandbergen PJ (eds), vol. 59. Springer: New York, 1976; 330–340.
45. Youngs DL. Time-dependent multi-material flow with large fluid distortion. In *Numerical Methods for Fluid Dynamics*, Morton KW, Baines MJ (eds). Academic Press: New York, 1982; 273–285.
46. Wang SP, Wang KK. A net inflow method for incompressible viscous flow with moving free surface. *International Journal for Numerical Methods in Fluids* 1994; **18**:669–694.
47. Van Leer B. Towards the ultimate conservative difference scheme. IV. A new approach to numerical convection. *Journal of Computational Physics* 1977; **23**:276–299.
48. Reddy JN, Gartling DK. *The Finite Element Method in Heat Transfer and Fluid Dynamics*. CRC Press: Florida, 1994.
49. Chorin AJ. Numerical solution of the Navier–Stokes equations. *Mathematics of Computation* 1968; **22**: 745–762.
50. Donea J, Giuliani S, Laval H, Quartapelle L. Finite element solution of the unsteady Navier–Stokes equations by a fractional step method. *Computer Methods in Applied Mechanics and Engineering* 1982; **30**:53–73.
51. Kim J, Moin P. Application of a fractional-step method to incompressible Navier–Stokes equations. *Journal of Computational Physics* 1985; **59**:308–323.
52. Ramaswamy B, Jue TC. Some recent trends and developments in finite element analysis for incompressible thermal flows. *International Journal for Numerical Methods in Engineering* 1992; **35**:671–707.
53. Choi HG, Choi H, Yoo JY. A fractional four-step finite element formulation of the unsteady incompressible Navier–Stokes equations using SUPG and linear equal-order element methods. *Computer Methods in Applied Mechanics and Engineering* 1997; **143**:333–348.
54. Kelly DW, Nakazawa S, Zienkiewicz OC, Heinrich JC. A note on upwinding and anisotropic balancing dissipation in finite element approximations to convective diffusion problems. *International Journal for Numerical Methods in Engineering* 1980; **15**:1705–1711.
55. Brooks AN, Hughes TJR. Streamline upwind/Petrov–Galerkin formulations for convection dominated flows with particular emphasis on the incompressible Navier–Stokes equations. *Computer Methods in Applied Mechanics and Engineering* 1982; **32**:199–259.

56. Martin JC, Moyce WJ. An experimental study of the collapse of liquid columns on a rigid horizontal plane. *Philosophical Transactions of the Royal Society of London*, *Series A. Mathematical*, *Physical and Engineering Sciences* 1952; **244**:312–324.
57. Maxworthy T. Experiments on collisions between solitary waves. *Journal of Fluid Mechanics* 1976; **76**:177–185.
58. Laitone EV. The second approximation to cnoidal and solitary waves. *Journal of Fluid Mechanics* 1960; **9**: 430–444.
59. Byatt-Smith JGB. An integral equation for unsteady surface waves and a comment on the Boussinesq equation. *Journal of Fluid Mechanics* 1971; **49**:625–633.

